13. Mass measurements in the isochronous rare-RI ring

List of collaborators

I.Arai, T.Komatsubara, H.Ohta, A.Ozawa, K.Sasa *(University of Tsukuba)*

M.Fujinawa, Y.Fukunishi, A.Goto, T.Ohnishi, H.Okuno, H.Sakurai, H.Takeda M.Wakasugi, M.Yamaguchi, Y.Yamaguchi, Y.Yano, (*RIKEN*)

T.Kikuchi (*Utsunomiya University*)

T.Suzuki, T.Yamaguchi (*Saitama University*)

T.Ohtsubo (*Niigata University*)

Abstract

We propose mass measurements for energetic RI beams with 200 *A* MeV using the isochronous ring. The isochronous ring allows us to determine the mass if we measure time-of-flight (up to 1ms) in the ring and velocity before the ring by combining individual injection. The uncertainty of the order of 10^{-6} will be achieved for the mass if we measure the velocity with the resolution of 10^{-4} and the momentum acceptance of the ring is the order of 10^{-2}. In order to measure velocity of the RI beams and to perform the individual injection, we need a long injection line up to ~190m. For the injection line, sector magnets and quadrupole magnets of heavy ion synchrotoron TARNII (77.8m of circumference) will be recycled. The isochronous ring consists of eight separate sectors with a bending angle of $\pi/4$ rad and eight identical straight sections (70m of circumference). Each sector has straight edges on its both ends to achieve isochronicity up to 10^{-4}. The harmonic field improves the isochronicity up to the order of 10^{-8}. Tuning of the isochronous ring should be done by stable nuclei with precisely known mass, which have the same m/q ratio as that of unstable nuclei to measure the mass in the ring. Isochronicity can be checked by accelerating the stable nuclei by RF with a low voltage in the ring. A kicker magnet is the important device to perform the individual injection and to extract the nuclei. To perform the individual injection for RI beams with 200 *A* MeV, fast response (~450 ns) is needed. Presently, response time of ~550 ns can be achieved. In the present system, angular and momentum acceptances of the isochronous ring (~10π-mm-mrad and ±1%, respectively) are much smaller than those of Big-RIPS (~100π-mm-mrad and ±3%, respectively). To overcome this problem, we propose individual trajectory correction

during the injection line, which consists of detectors for angular spread of RI beams and fast electric kickers. This system allows to decrease angular spread of RI beams by event-by-event mode and to increase RI beam intensity in the isochronous ring by the several factors.

Contents

Introduction

1.1 Overview

We propose a new scheme of precise mass measurements matching energetic RI beams with 200 *A* MeV produced via primary beams from the cyclotron complex of RIBF. To exploit the potential of the RIBF facility as much as possible, we adopt a particle-by-particle injection to and extraction from a ring designed to have the isochronous optics. The use of the isochronous optics is essential to give us great access toward short-lived nuclei far from the stability line. In addition to measure time-of-flight of particles in the ring, particle velocity before the injection (in the injection line) is measured to correct the isochronous condition. Due to the velocity measurement, a mass accuracy of 10^{-6} will be achieved for a wide momentum acceptance of ~10^{-2}. Individual injection/extraction also allows us to identify the RI beams event-by-event. The identification brings out nice signal/background ratios.

1.2 Physics interests

Mass measurements of unstable nuclei are essential for studies of nuclear structure, allowing us to discover new shell effects, nuclear shapes and decay properties. Precision mass measurements are also crucial tests for nuclear models. Moreover, mass measurements are important to determine the astrophysical *r*-process path, which is only predicted one based on existing mass formulae. In RI beam factory (RIBF), very intense energetic RI beams, including unknown mass region, are available by projectile fragmentation process and/or uranium fission. Thus, we propose mass measurements for the energetic RI beams in RIBF.

1.3 Experimental requirements

At first we present principle of measurements. We start from cyclotron frequency in the ring. Frequency in the storage-ring can be given by so called cyclotron frequency (f_c), as shown in

$$f_C = \frac{1}{2\pi}\frac{qB}{m} , \qquad (1.1)$$

where m/q is mass-to-charge ratio of particle in the ring and B is magnetic field of the ring. Thus, circulation time in the ring (T) is obtained by reversing Eq. (1.1),

$$T = 2\pi \frac{m}{q} \bullet \frac{1}{B} = 2\pi \frac{m_0}{q} \bullet \frac{1}{B} \bullet \gamma, \qquad (1.2)$$

where $\gamma = 1/\sqrt{1-\beta^2}$, β=v/c and c is the light velocity. In the isochronous ring, B becomes $B_0\gamma$ at certain m_0/q. Thus, we obtain the following equation for the certain m_0/q,

$$T_0 = 2\pi \frac{m}{q} \bullet \frac{1}{B} = 2\pi \frac{m_0}{q} \bullet \frac{1}{B_0} \qquad (1.3)$$

For RI beams with different mass-to-charge ratios $((m_1/q)=m_0/q+\Delta(m_0/q))$, isochronism is not fulfilled. In this case, mass-to-charge ratio can be given by

$$\frac{m_1}{q} = \left(\frac{m_0}{q}\right)\frac{T_1}{T_0}\frac{\gamma_0}{\gamma_1} = \left(\frac{m_0}{q}\right)\frac{T_1}{T_0}\sqrt{\frac{1-\beta_1^{\,2}}{1-\left(\frac{T_1}{T_0}\beta_1\right)^2}}, \qquad (1.4)$$

where T_1 is circulation time for nuclei with m_1/q and $\gamma_1 = 1/\sqrt{1-\beta_1^{\,2}}$. Thus, to evaluate the mass of nuclei with non-isochronism, we need correction of velocity (β). Relative differential of m_1/q is given by

$$\frac{\delta\left(m_1/q\right)}{m_1/q} = \frac{\delta\left(m_0/q\right)}{m_0/q} + \frac{\delta\left(T_1/T_0\right)}{T_1/T_0} + k\frac{\delta\beta_1}{\beta_1} \qquad (1.5)$$

$$k = \frac{\beta_1^2}{1-\beta_1^2} - \left(\frac{T_1}{T_0}\right)^2 \frac{\beta_1^2}{1-\left(T_1/T_0\right)^2\beta^2} \qquad (1.6)$$

Accuracy of the mass depends on the accuracy of the velocity. If we require the order of 10^{-6} mass accuracy, the third term in Eq. (1.5) should be less than 10^{-6}. 10^{-2} difference of the mass (i.e., $\Delta(m_0/q)/(m_0/q)$~10^{-2}) corresponds to ~10^{-2} difference of circulation time and k~10^{-2}. Thus, if we determine velocity with 10^{-4} accuracy, the third term in Eq. (1.5) becomes around 10^{-6}. In summary, for RI beams with non-isochronism we can use Eq. (1.4) to determine the mass. 10^{-6} mass accuracy can be achieved even for RI beams with 10^{-2} difference of the mass if we measure the velocity with 10^{-4} accuracy.

1. Experimental setup

1.1 Overview

We propose a scheme as shown in Fig. 2.1 for the mass measurements in the ring. As described in Sec. 1, we need to measure the circulation time with 10^{-6} accuracy, and velocity with 10^{-4} accuracy. In order to measure velocity of the RI beams, we need a

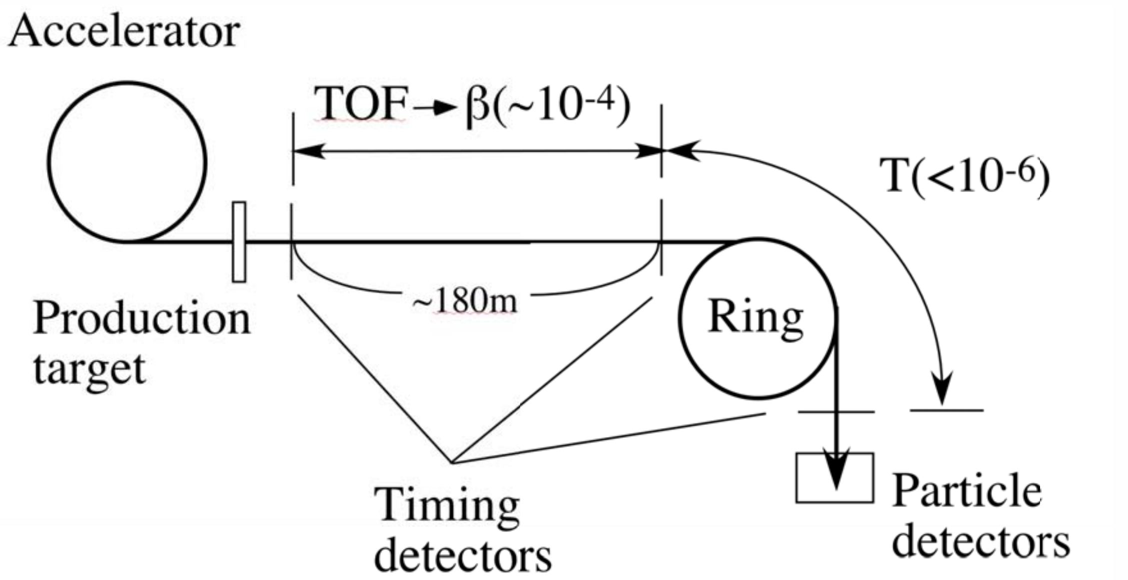

Fig. 2.1 A conceptual drawing for scheme of mass measurements for short-lived RI beams.

long injection line. We can achieve 100 ps time-resolution that can be obtained by conventional timing detectors. Thus, for 1 μs flight time, we can achieve 10^{-4} accuracy for the time-of-flight (TOF). 10^{-4} accuracy of TOF can provide ~10^{-4} accuracy of the velocity. 1 μs flight time corresponds to ~180 m flight-length for the RI beams with 200 *A* MeV. According to Eq. (4), accuracy of the circulation time directly affects accuracy of the mass. If we assume 100 ps time resolution, the circulation time should be more than 100 μs to achieve the 10^{-6} accuracy. If we assume the ring with the circulation time of 300 ns/turn, 10^{3} turns in the ring are needed. In this scheme, we do not count the circulation number, however, we know the velocity of the RI beams with 10^{-4} accuracy before the ring. We do not miss the number of circulation in the ring.

In this scheme, event-by-event velocity measurements are indispensable. Such measurements can be done individual injection proposed by Ref. [2.1]. Individual injection also allows us to identify the RI beams; $B\rho$ and velocity give A/q, ΔE and velocity give Z, and total E and velocity give A, respectively. Thus, scheme in Fig. 2.1 provides complete particle identification for the RI beams.

2.2 Isochronous storage ring

2.2.1 Structure and Design Principles

To achieve 10^{-6} accuracy of the mass, isochronicity inside the ring should be less than 10^{-6}. The isochronous ring consists of eight identical separate sectors with a bending angle ϕ of $\pi/4$ rad and eight identical straight sections. Each sector has straight edges on its both ends. The edges are tilted by the edge angle β from the normal to the central orbit so that their opening angle θ becomes reduced to $(\phi - 2\beta)$. The magnetic field in each sector has two components, i.e., (1) the uniform field B_0 produced by the main coil and (2) the harmonic field B_h produced by a set of trim coils.

The basic design principles are as follows;

1) The dispersion matching injection is adopted.

2) The edge angle β is introduced in order to cancel the deviation from isochronicity condition in the first order of $\Delta p / p$.

3) The harmonic field B_h is applied in order to cancel the deviation from isochronicity condition in the second order of $\Delta p / p$.

Under the dispersion matching injection and the edge angle β, the isochronicity of about 10^{-4} is achieved over the range of $\Delta p / p$ from -1% to +1%. The harmonic field further improves the isochronicity up to about 10^{-8}.

For dispersion matching, the beam particle with a momentum of $(p + \Delta p)$ should enter at the following position on an entrance edge of the first magnetic sector

$$x_{\Delta p} = \left\{ \frac{1}{2\tan\frac{\phi}{2}} \left[S - (R\phi + S)\beta^2 \right] + R \right\} \frac{\Delta P}{P} \tag{2.1}$$

$$s_{\Delta p} = \frac{\left[S - (R\phi + S)\beta^2 \right]}{2} \frac{\Delta P}{P} \tag{2.2}$$

where the coordinate system refers the entrance point on the central orbit as $x = 0$ and

$s = 0$.

Under the dispersion matching injection, the appropriate edge angle β is given by the following formula by taking into account the shift of both the velocity of beam particle and its γ factor in the first order of $\Delta p / p$.

$$\beta = \tan^{-1}\left\{ \frac{\tan\frac{\phi}{2}\left[S - (R\phi + S)\beta_C{}^2\right]}{\left[S - (R\phi + S)\beta_C{}^2\right] + 2R\tan\frac{\phi}{2}} \right\} \qquad (2.3)$$

where S and R are the length of straight section and the radius of central orbit, respectively, while β_C is the velocity of beam particle on the central orbit in units of c.

The harmonic field B_h is dependent only on the radial coordinate x and defined as

$$B_h = B_0(1 + \alpha\kappa x^2) \qquad (2.4)$$

where κ and α are a second order coefficient and a correction factor, respectively. The second order coefficient κ is given by the formula

$$\kappa = \frac{\left(1 + \frac{S}{R\phi}\right)\beta_C{}^2(1 - \beta_C{}^2)}{\left\{ \frac{1}{2\tan\frac{\phi}{2}}\left[S - (R\phi + S)\beta_C{}^2\right] + R \right\}^2} \qquad (2.5)$$

The correction factor α has a value in the range from 0 to 1, which is dependent mainly on the edge angle β.

For a non-zero value of the edge angle β, the effect of edge focusing is evaluated based on a hard edge approximation as follows;

$$\Delta x' = -\tan\beta \frac{x - x_{\Delta p}}{R\left(1+\frac{\Delta p}{p}\right)\gamma}$$

(2.6)

$$\Delta y' = \quad \tan\beta \frac{y}{R\left(1+\frac{\Delta p}{p}\right)\gamma}$$

(2.7)

The design flow is as follows. At first, the energy of beam particle on the central orbit is determined as 200 *A* MeV from the experimental requirement. Then, the velocity β_C becomes 0.567690. Under the constraint on the possible range of magnetic rigidity, the radius of central orbit is determined as 4.2m. Both the number of sectors and the circumference of central orbit are determined as 8 and 70m, respectively, under the condition which gives the vertical and horizontal betatron oscillations with desirable tunes. Finally, the correction factor α for the harmonic field is optimized to obtain the maximum emittance. The design proceeds with the help of computer simulation.

2.2.2 Computer Simulation

The computer simulation program is coded in C language. It consists of five components, i.e., 1)main.c, 2)Ring.c, 3)ST.c, 4)DM.c and 5)Eq.c. The program main.c handles setup parameters for the desirable ring. The parameters are as follows;

1) Number of magnetic sectors
2) Circumference of central orbit
3) Radius of central orbit
4) Velocity of beam particle on the central orbit in units of *c*
5) Charge to mass ratio of beam particle

With these parameters, a database for actual dimensions of the ring and its excitation are automatically determined. The database is transferred to the program Ring.c which controls each element of the ring and rotates beam particles 1000 times along their orbits. The program ST.c represents a straight section while the program DM.c a magnetic sector.

To achieve the precision as high as possible required for determination of the trajectory of beam particle, we adopt a geometrical tracking in the magnetic sector under assumption of a circular orbit for a given small spatial duration. For this purpose, a magnetic sector is divided into 100 sub-sectors conceptually. In each sub-sector, the magnetic field B_κ is fixed to a predetermined value following to the trajectory itself. When the beam trajectory at the entrance of sub-sector is given by (x, x', y, y', s), the corresponding four beam trajectories at its exit are evaluated successively in association with different B_κ's as follows;

1)evaluate $(x_1, x_1', y_1, y', s_1)$ based on $B_\kappa(x, s)$
2)evaluate $(x_2, x_2', y_2, y', s_2)$ based on $B_\kappa((x + x_1)/2, (s + s_1)/2)$
3)evaluate $(x_3, x_3', y_3, y', s_3)$ based on $B_\kappa((x + x_2)/2, (s + s_2)/2)$
4)evaluate $(x_4, x_4', y_4, y', s_4)$ based on $B_\kappa(x_3/2, s_3/2)$

It should be noted that y' remains constant in the above evaluations. Finally, the actual beam trajectory $(x_e, x_e', y_e, y_e', s_e)$ at the exit is given by a weighted mean of four evaluations, i.e.,

$$x_e = \frac{1}{6}\left(x_1 + 2x_2 + 2x_3 + x_4\right)$$
$$x_e' = \frac{1}{6}\left(x_1' + 2x_2' + 2x_3' + x_4'\right)$$
$$y_e = \frac{1}{6}\left(y_1 + 2y_2 + 2y_3 + y_4\right)$$
$$y_e' = y'$$
$$s_e = \frac{1}{6}\left(s_1 + 2s_2 + 2s_3 + s_4\right)$$

The procedure entirely corresponds to a 4th order Runge-Kutta algorithm.

2.2.3 Isochronicity and available emittance

The currently used optimum parameters are listed in Table 2.1. In the present parameters, vertical tune is very close to 1. Further refinement will avoid this resonance point. Carrying out computer simulations with use of these parameters, the resulting isochronisities on the x-x' plane are examined in view of 3-D contour map. A typical 3-D contour map for $\Delta p / p = +1\%$ is shown in Figure 2.2. It is found that an emittance of a few π mm mmrad is available under requirement of the isochronicity better than 10^{-7}. Figure 2.3 shows a variation of the available emittance as a function of $\Delta p / p$. At least, a few π mm mmrad is available in the whole range of $\Delta p / p$. It is noted that momentum dependence of emittance has a asymmetrical shape. This asymmetry may be due to third order effects of the harmonic field.

Table 2.1 : Storage Ring Main Parameters

Injection Energy	200 [*A* MeV]
Particle Velocity	0.567689 [c]
Circumference	70 [m]
Straight Sections	5.451328 [m/Unit]
Sectors 1) Number of Units 2) Radius of Curvature 3) Bending Angle 4) Edge Angle 5) Radial Width 6) Magnetic Fraction 7) κ	 8 [Units] 4.2 [m] 0.78540 [rad] 0.176512 [rad] 0.432374 [rad] 0.550516 0.00850 [/m^2]
Horizontal Tune	1.255
Vertical Tune	1.003

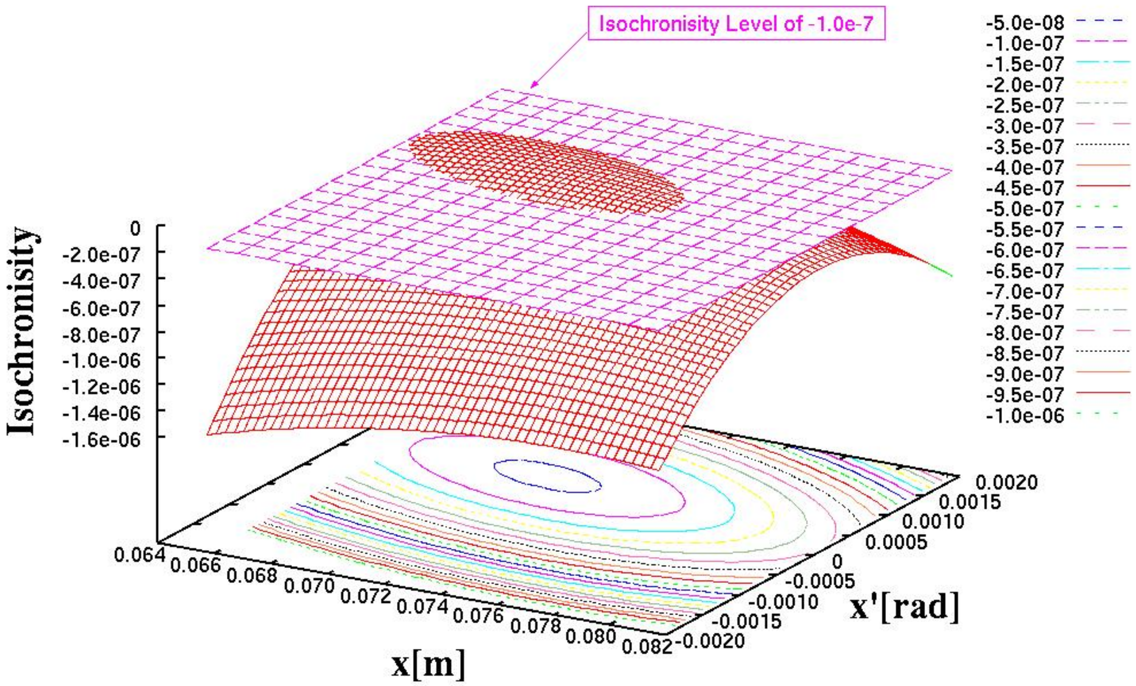

Fig. 2.2 A typical 3-D contour map for $\Delta p / p = +1\%$ in the isochronous storage ring.

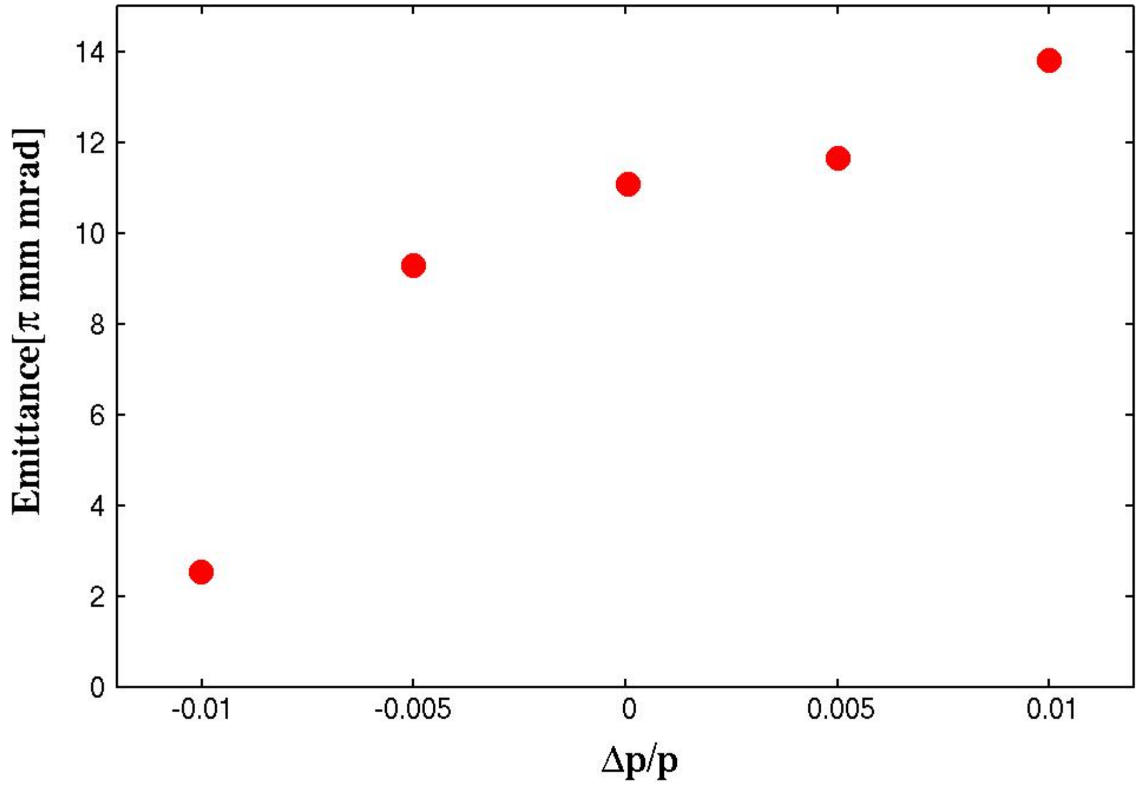

Fig. 2.3 A variation of the available emittance as a function of $\Delta p / p$.

2.2.4 Tuning of the isochronous storage ring

Here we describe tuning procedure for the storage ring. Tuning should be done by nuclei with precisely known mass. In this sense, it is preferable to tune by stable nuclei, where the masses are known precisely with the accuracy of less than 1 keV.

In the RIBF cyclotron complex, various stable nuclei with different energies can be accelerated up to 200 *A*MeV. After the tuning, any

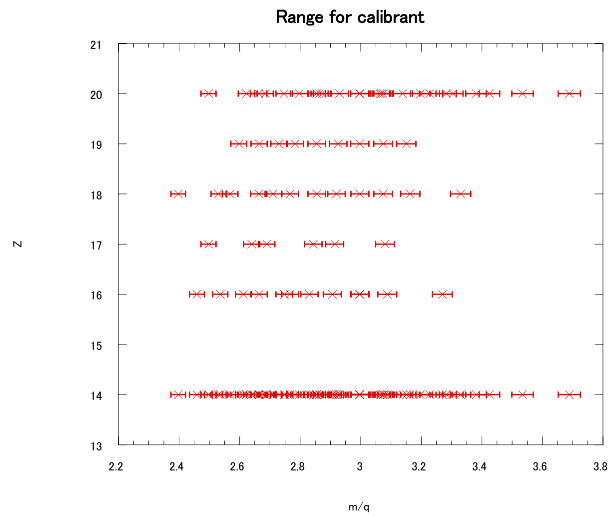

Fig. 2.4 m/q of the stable nuclei, which can be accelerated in the RIBF cyclotron complex up to 200 *A*MeV.

magnetic field should not be changed since isochronous field is broken by any change of magnetic fields. If we measure the mass of neutron rich unstable nuclei, *m/q* becomes large up to 3. Thus, stable nuclei with large *m*/*q* number should be accelerated and injected to the storage ring. The stable nuclei which can be accelerated up to 200 *A*MeV in RIBF are shown in Fig. 2.4. In Fig. 2.4, error bars of X-axis show ±1% acceptance of *m*/*q*, which corresponds to momentum acceptance of storage ring. Thus, the stable nuclei to be accelerated in RIBF can cover $2.4<m/q<3.4$ continuously.

Tuning of isochronicity in the storage ring should be noted. Isochronicity is fulfilled if TOF in the storage ring is the same for the nucleus with different momentum (up to ±1%). However, in the cyclotron, only small change of momentum ($\sim10^{-3}$) is possible. If we install any degrader to change the energy of stable beam during the injection line, charge state of the stable beam will change close to its own *Z* in 200 *A* MeV. Thus, *m/q* of the stable nuclei will be close to 2 and the stable nuclei can not be injected to the ring. To overcome this problem, some acceleration of the stable nuclei inside the storage ring is needed. The variations of magnetic field (*B*) are directly related to the variations of ToF in the ring (*t*) and total phase (Φ), as follows.

$$\frac{\delta B}{B} = \frac{\delta t}{t} = \frac{\delta \Phi}{\Phi} \qquad (2.8)$$

ToF can be given by

$$t = T_{\mathrm{HF}} \times h \times N_{\mathrm{T}}, \qquad (2.9)$$

where h is the beam harmonic and N_{T} is turns at harmonic h, respectively. Thus, variations of magnetic field is given by

$$\frac{\delta B}{B} = \frac{\delta t}{T_{HF} \times h \times N_T} \qquad (2.10)$$

If the time resolution of timing detector is 0.1 ns and $N_t \sim 10^3$, variations of magnetic field can be down to 10^{-6}. Thus, isochronicity can be checked up to 10^{-6} in this case. Since variations of energy are very small in the ring (±2%), voltages of RF will be smaller than that used in present cyclotrons in RIBF.

2.3 Kicker and septum for the isochronous storage ring

2.3.1 R&D for kicker magnet

A kicker magnet is one of the most important devices, because it is used for beam injection to and extraction from a synchrotron and a storage ring. We construct a storage ring (isochronous ring) for precise mass measurement, so the best kicker magnet for the specification of our isochronous ring is necessary.

We fortunately have a model kicker magnet system, which was made for a former project in RIKEN [2.2,2.3], and by using a model system we are performing R&D of the following two issues;

1 Possibility of a high-speed response of the kicker magnet power supply,

2 Optimization of the magnetic field waveform.

2.3.1.1 High-speed response of the kicker magnet

A distance of 190 m between trigger detector and kicker magnet at the injection line corresponds to about 1120 ns flight time for 200*A* MeV particles. Accordingly, it is necessary to make the trigger signal transmitted to the kicker magnet earlier than the above-mentioned time, in order to inject the beam into the isochronous ring by using the kicker magnet. Figure 2.5 indicates the expected time of the trigger signal transmission and the route.

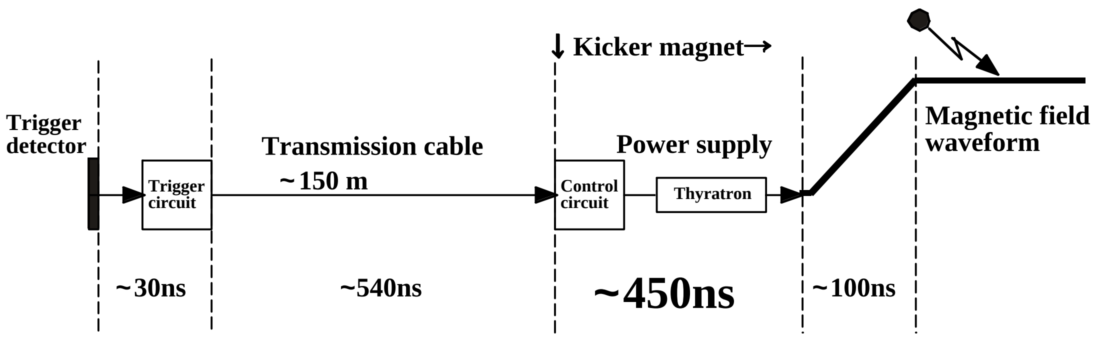

Fig. 2.5 The time of the trigger signal transmission and the route

We use a plastic scintillator set up as the trigger detector at the F3 focal plane of BigRIPS [2.4]. Transmission time of the trigger signal up to the kicker power supply is about 570 ns, while a rise time of the magnetic field is typically about 100 ns, as shown in Fig. 2.5. Therefore, it is necessary to achieve a short operation time of 450 ns or less at the start-up device for our kicker magnet. This is crucial point for our injection system. Thus, we should be verifying how much the operation time could be shortened by using the power supply of the model kicker magnet.

The power supply of the model kicker magnet consists of the pulse forming network (PFN), the thyratron and the termination. Fig. 2.6 is a schematic diagram of the power supply and the transmission time of electrical discharge trigger signal (DT1).

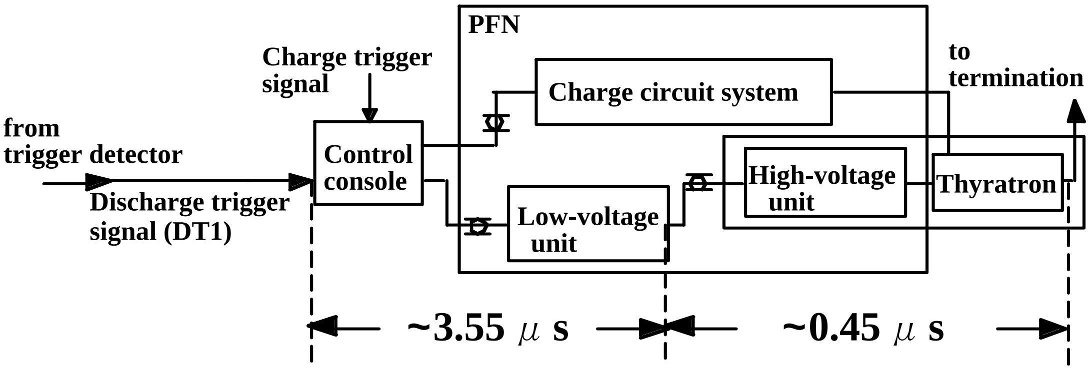

Fig.2.6 Schematic of the power supply and the transmission time of electrical discharge trigger signal (DT1).

The transmission time of DT1 is about 4.0 μ s, when the PFN voltage is charged with 8 kV under the present condition. What should we do to improve this part at about 450 ns ? We just started verification whether this value is able to be achieved or not.

At the first step the electrical discharge trigger signal (DT2) is newly added to present system, and it is input directly to the high-voltage unit, as shown in Fig. 2.7.

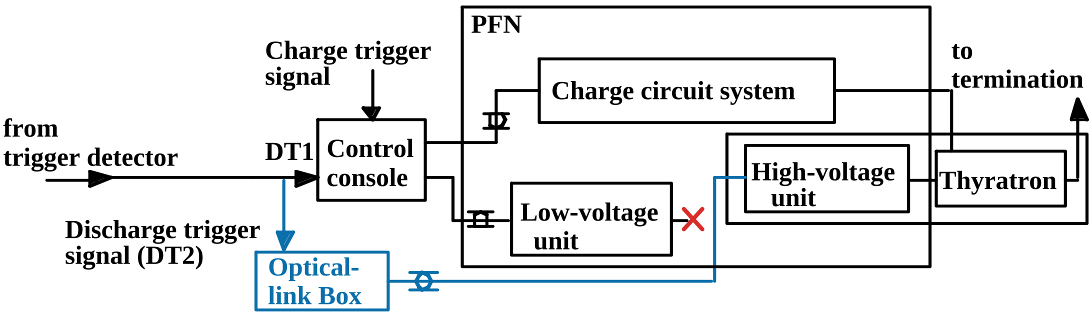

Fig.2.7 Schematic of the power supply after the first step remodel.

Because DT2 line is not passing through the Control console and the Low-voltage unit, it should be transmitted with about 450 ns from DT2 input timing to thyratron output timing at the PFN charging voltage of 8 kV. Recently, we measured the transmission time of DT2. It was about 615 ns at the PFN charging voltage of 8kV. Unfortunately, the cause of the difference of both is not understood up to now. We also measured the PFN voltage dependency. The results are shown in Fig. 2.8.

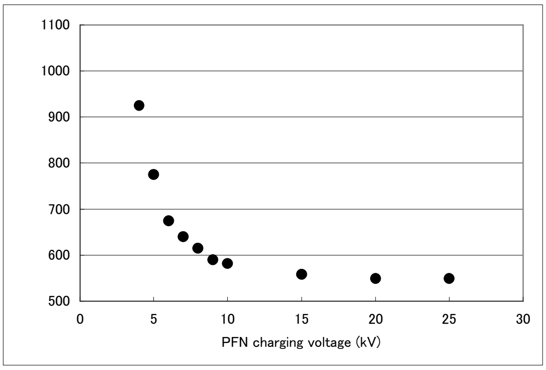

Fig.2.8 Transmission time as a function of the PFN charging voltage.

The transmission time was saturated in the vicinity of about 20kV, and it was about 550 ns. As a result of this first step, the operation time of the start-up device has been improved from 4.0 μ s to 550 ns. However, it does not reach 450ns still and a further improvement is necessary.

At the second step, we are improving the high-voltage unit, speed-up of all optical-link system and so on. This step has not been done yet. We are convinced that it can be achieved through discussions with technical experts in details.

2.3.1.2 Magnetic field waveform of the kicker

The kicker magnet must generate high magnetic field with rapid rise and hall time, and make a uniform flattop for an efficient injection. Concerning our system, an ideal waveform of magnetic field for injection kicker magnet is shown in Fig. 2.9.

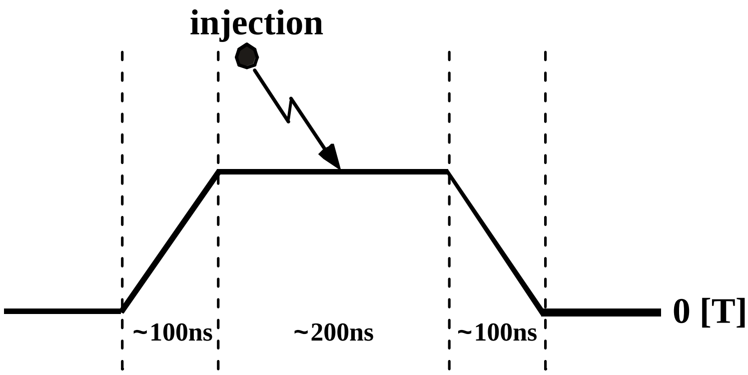

Fig.2.9 Ideal waveform of magnetic field for injection kicker magnet.

The rise and fall time of waveform would be achieved at less than 100 ns. The flattop time about 200 ns with proper magnetic field strength, because an incidence beam has a few time-dispersion and passes the same place after 400 ns, as described in Sec. 2.2, and therefore it is necessary to adjust the magnetic field to 0 T completely after one rotation.

Realistically speaking, a ringing influences the shape of waveform. The ringing is due to the reflection caused by the mismatch of impedance. We can adjust a matched resistance in order to decrease the ringing as much as possible. Tolerance for amplitudes of ringing depends on the specification of our injection scheme, beam emittance and so on. Though this R&D is scheduled after making a new kicker magnet for the isochronous ring, it is clear that it becomes easy to approach the ideal waveform by doing similar work using the model kicker magnet beforehand.

2.3.2 Injection scheme

We adopt a single-turn injection scheme. In the single-turn injection, the beam is brought onto the central orbit of the isochronous ring using a septum and a kicker magnet. Aim of the injection scheme design is to achieve minimum beam loss and beam emittance dilution. For the isochronous ring, the dispersion matching as well as the emittance matching at an injection point might be indispensable. The preliminary technical layout of the injection scheme is shown in Fig. 2.10.

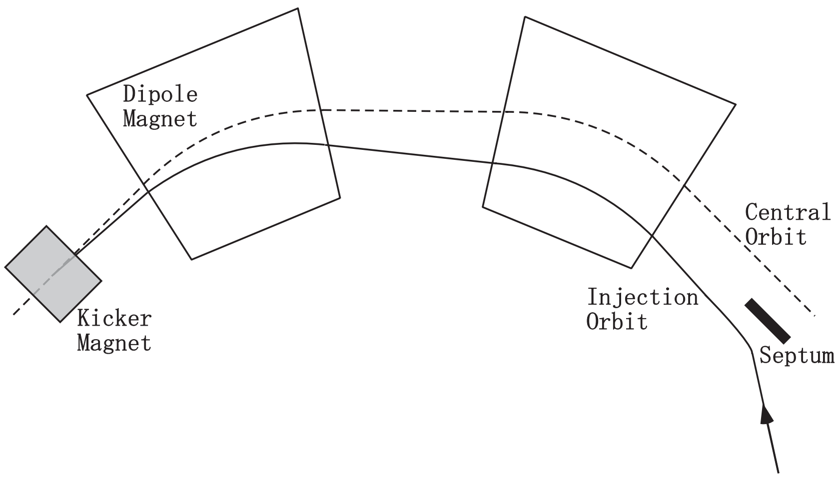

Fig.2.10 Conceptual drawing of
the injection scheme.

The phase advance from the septum to the kicker magnet is $\pi/2$. A large value of beta function at the kicker magnet reduces the kicker magnet strength. Based on the injection scheme, we are determining detailed specifications of the septum and kicker magnets.

2.3.3 Fundamental specifications

We simulated the TWISS parameter for our isochronous ring by using MAD program and provided a certain beam condition, as shown in Table 2.2.

ITEM	@SEPTUM	@KICKER	NOTE*
β_x	β_1=7.0[m]	β_2=7.0[m]	$\beta_x=\beta_1=\beta_2$
α_x	α_1=0.0	α_2=0.0	$\alpha_x=\alpha_1=\alpha_2$
Dispersion	D_x =5.8[m]		-------
Beam emittance; 10 π [mm·mrad]			
Momentum acceptance; +/- 1.0[%]			

Table2.2 TWISS parameter for our isochronous ring and a certain beam condition.

*Septum and kicker magnet are set up at a center of straight section.

Under this condition, a distance x_1 between central-orbit and injection beam in horizontal direction at the exit of the septum is assumed about 160 mm. An angle x_1' of injection beam at the exit of the septum is assumed 0 mrad. Then, this injection scheme is considered on the phase space coordinates, as shown in Fig. 2.11.

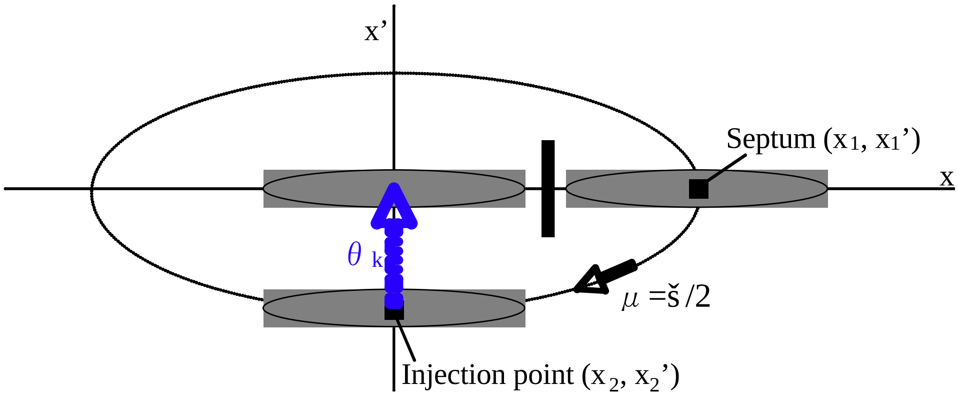

Fig.2.11 Phase space coordinates of the injection scheme.

The injection beam must be at the center of the central-orbit when it reaches the kicker magnet so that the x_2 equal to 0 mm. An angle x_2' (= θ_k) was calculated by using the following transfer matrix (M_{12}):

$$M_{12} = \begin{pmatrix} \sqrt{\frac{\beta_2}{\beta_1}}(\cos\mu + \alpha_1 \sin\mu) & \sqrt{\beta_1\beta_2}\sin\mu \\ -\frac{1}{\sqrt{\beta_1\beta_2}}((1+\alpha_1\alpha_2)\sin\mu + (\alpha_2 - \alpha_1)\cos\mu) & \sqrt{\frac{\beta_1}{\beta_2}}(\cos\mu - \alpha_2\sin\mu) \end{pmatrix}, \qquad (2.11)$$

where μ is a phase advance equal to $\pi/2$ mentioned above. Here, TWISS parameter in Table 2.2 is substituted for this transfer matrix. Then, the injection point (x_2 , x_2') is calculated by using following equation:

$$\begin{pmatrix} x_2 \\ x_2{}' \end{pmatrix} = M_{12}\begin{pmatrix} x_1 \\ x_1{}' \end{pmatrix} = \begin{pmatrix} 0 & \beta_x \\ -\beta_x{}^{-1} & 0 \end{pmatrix}\begin{pmatrix} x_1 \\ x_1{}' \end{pmatrix}, \qquad (2.12)$$

and the result was x_2' (= θ_k) = 23 mrad. The magnetic field strength B_k = 0.061 T could be calculated from $B_k = (B\rho \cdot \theta_k) / L$, where $B\rho$ is a magnetic rigidity of beam and L is a total core length of the kicker magnet, which are given in Table 2.3.

Table 2.3 shows the fundamental specifications of kicker magnet. The concept is an equal ability with a model kicker magnet.

TYPE; Traveling wave type		
ITEM	DESIGN VALUE	
Magnetic rigidity of beam	$B\rho$ = 6.4[Tm]	
Total core length	L = 2.4[m]	
Aperture	Height; 40[mm]	Width; 200[mm]
Rise and fall time	~100[ns]	
Kick angle	θ_k = 23[mrad]	
Kicker magnet strength	B_k =0.061[T]	
Characteristic impedance	25[Ω]	
Current	1941[A]	
PFN voltage	98[kV]	
Total number of unit kicker	12	
Kick angle of unit kicker	1.9[mrad]	
Cell number of unit kicker	8	
Inductance of unit cell	157[nH]	
Capacitance of unit cell	251[pF]	

Table2.3 The fundamental specifications of the kicker magnet.

We have confirmed the fundamental specifications of the kicker magnet under an ideal injection condition. This is guideline for next detail discussion, which based on a more realistic condition with the septum and other injection line devices. In addition, we will discuss an extraction scheme, which is roughly the reverse process of injection scheme.

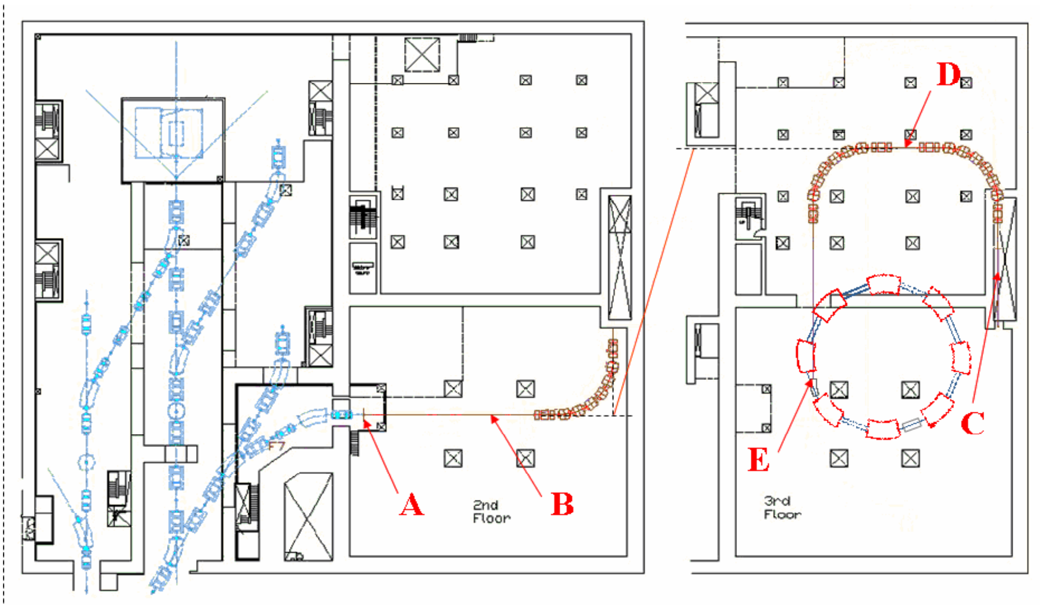

Fig.2.12 Layout of the injection line and the storage ring.

2.4 Injection line from BigRIPS to the ring

In Fig. 2.12, present design of the injection line and isochronous storage ring is presented. There are several limitations to design a disposition of devices. In actual construction, we recycle the magnets of TARN-II [2.5], which was constructed for Heavy ion Cooler Synchrotron. The maximum rigidity of TARN-II is 6.1Tm, which is determined by maximum dipole magnetic field of 1.5T. Thus, because of the limitation of the power supply, the maximum rigidity of injection line is limited as 6.1Tm, however, that can be excited up to 7.3Tm in future. The BigRIPS line comes from left-hand side of Fig. 2.12 on **B2F**, and connects to our injection line. Since the isochronous ring will be constructed on **B1F** in our present plan, we have to consider such design as the injection line goes upstairs to **B1F** from **B2F**. Therefore, we make double-achromatism and parallel beam at **B** and **D** so that the injected beam makes parallel bundle and we can twist injection line at **B** and **D**. Furthermore, to prevent from spreading the beam in dipole magnets, we squeeze radius of the beam by quadrupole triplets. Through the hole placed at right-hand side of Fig.2.12 on **B1F**, the injection line is lifted up to **B1F** straightly. For the injection to the storage ring, dispersion matching is indispensable to maintain good mass resolution and good transmission during circulation. Thus, we make the beam dispersive at the septum magnet placed at the entrance of the storage ring.

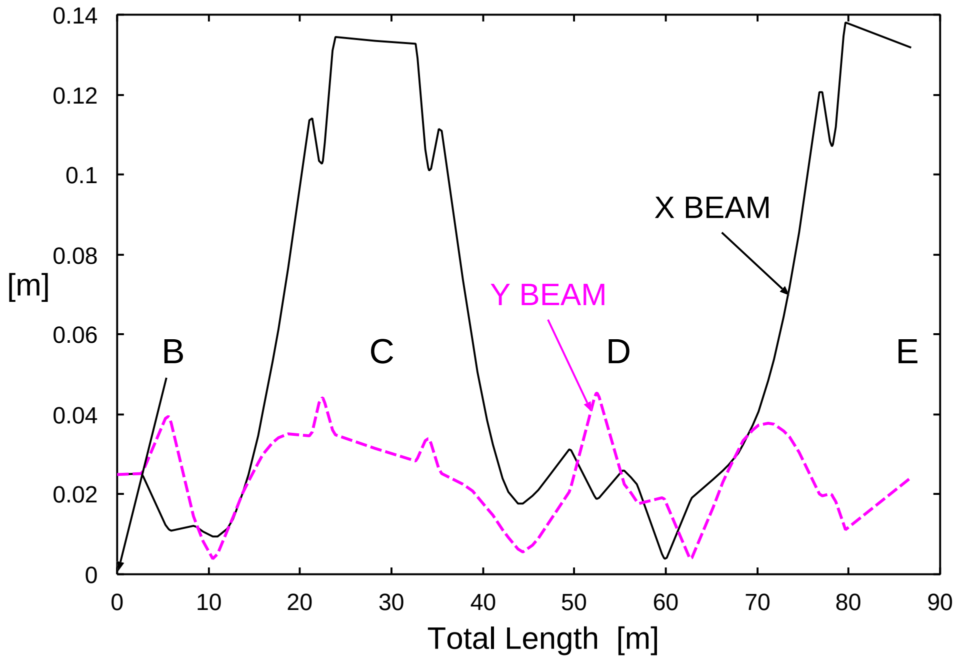

Fig.2.13: Calculated beam radius. Beam acceptances of both x- and y-directions are 25 π mm-mrad and momentum dispersion is about 1%

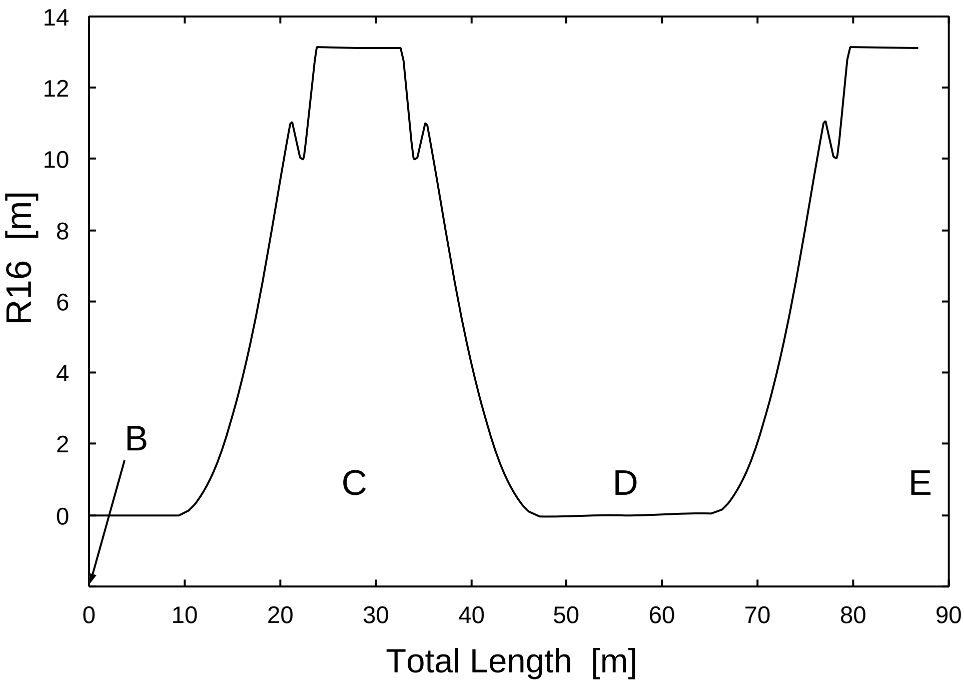

Fig.2.14: R16 element of transfer matrix

We made a simulation using the computer code TRANSPORT with the condition above. Here, we assume 200*A*MeV as the energy of the injected beam. The calculated result of the beam radius is represented in Fig. 2.13. We also show the result of R16 element of the transfer matrix in Fig. 2.14. As we expected, double-achromatism is achieved at **B** and **D**, and the injected beam makes tolerable parallel bundle. Calculated beam acceptance is about 25 π mm-mrad and momentum dispersion is about 1%. The total length of the injection line, **A-E**, is about 103*m*.

3. Upgrade program

3.1 Individual Trajectory Correction of RI

After BigRIPS, RI beam has a large emittance and a large momentum spread. Since storage ring for mass measurements has a finite acceptance, the RI storage rate decreases. To increase the efficiency, the large emittance and the large momentum spread should be decreased into the acceptable values of the storage ring.

The individual trajectory correction method, which was proposed by Meshkov, et al. [2.1], has possibility of emittance reduction of RI beams with low flux. The method consists of simple procedures as mentioned in next section. The scheme is described, and the parameter values required are estimated. Also, selected momentum correction method [3.1] is introduced for low flux rare RI beam with a large momentum spread.

3.1.1 Individual Trajectory Correction Scheme

Figure 3.1 shows scenario of the individual trajectory correction method.

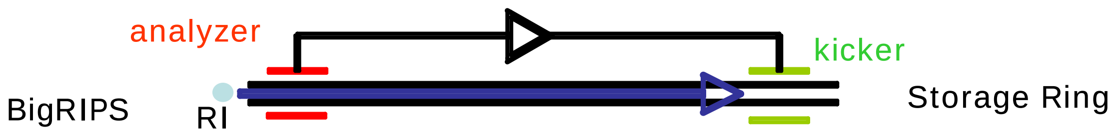

Fig.3.1: System of individual trajectory correction.

An analyzer individually detects the single RI particle, and the correction angle is calculated. The RI signal can trigger an electrostatic kicker. The electrostatic kicker generates electric field in the gap of electric plates. The electric field generated can be controlled by voltage adder system, which consists of pulsed-power devices. The electric field generated can individually kick the RI, and the RI trajectory is corrected.

RIKEN PPAC [3.2] is a candidate of the analyzing device, and the device can operate with accurate resolutions and fast response for the RI position detection. A typical response time of the PPAC is about 30ns. For this reason, the analyzer will be able to produce trigger signal for kicker operations.

In this report, we should consider on the electrostatic kicker and the voltage adder system.

3.1.2 Pulse Power System for Electro-static Kicker

Based on pulsed-power device, the electrostatic kicker can be operated with fast rise and fall voltage pulse. Fig. 3.2 shows an equivalent circuit of the pulser [3.3].

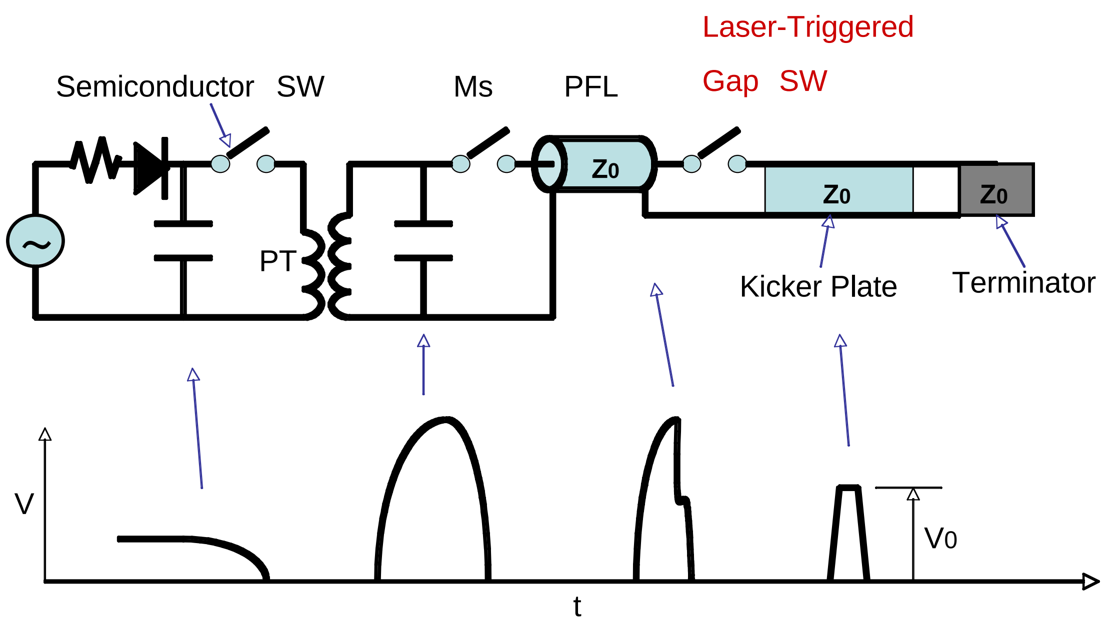

Fig.3.2: Voltage adder system based on pulsed-power technology and typical voltage waveform at each section. PT means a pulse transformer, Ms is a magnetic switch and PFL is a pulse forming line, respectively.

In this example, capacitance system accumulates the charge as shown in the left side region of Fig.3.2. In this stage, the operation voltage is low, so that the semiconductor switch is useful device. The accumulated charge is transferred into the middle stage by using pulse transformer, and the voltage is increased in this region. Magnetic switch (Ms) feeds the charge into pulse forming line (PFL). The PFL can transform the pulse shape transferred from the PFL. Gap switch is a candidate as switching device to fire the kicker. If laser-triggered gap switch is used, the switching time may be less than the order of nsec. The trigger for the kicker operation is from the analyzer.

3.1.3. Electrostatic kicker with fast pulse operations

3.1.3.1 Key issues

The key issues are (1) high voltage required for the RI kick and (2) lifetime of the gap switch. From the viewpoint of physics issue, the breakdown voltage restricts the electric field between the kicker plates.

3.1.3.2 Basic equations and relation

Figure 3.3 shows the kicker plate system.

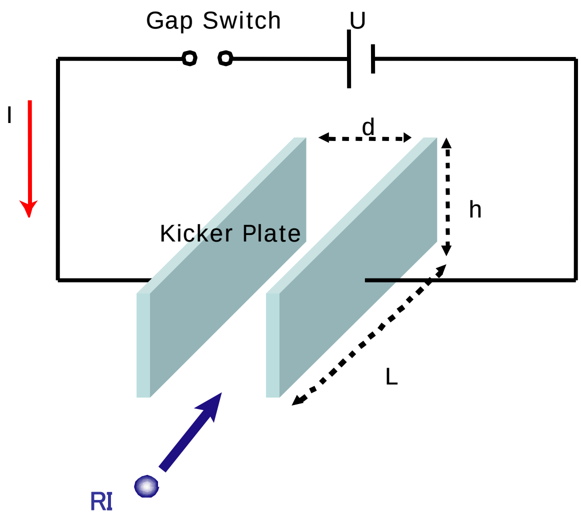

Fig.3.3: Electrostatic kicker system.

For the trajectory correction angle ϕ, the electric field E is required by

$$E = \frac{Am_p c^2 \beta^2 \gamma \phi}{ZeL}, \qquad (3.1)$$

where A is the mass number, $m_p c^2$=938MeV, β is the velocity divided by light speed c, γ is the relativistic factor, Ze is the charge of the RI, L is the electric plate length, respectively.

The required voltage U is given as

$$U = Ed, \qquad (3.2)$$

where d is the distance between the plates.

The lifetime of the gap switch for the kicker operation depends on the charge passed in the gap. The limitation shot number N_s of the gap switch is estimated by

$$N_s = \frac{Q_l}{Q_s}. \qquad (3.3)$$

Here Q_l is the limitation charge in gap switch and Q_s is the passage charge per one shot.

The charge per one shot is calculated by

$$Q_s = CU, \qquad (3.4)$$

where C is the electrical capacitance of the kicker plate,

$$C = \frac{\varepsilon_0 hL}{d}. \qquad (3.5)$$

Here h is the plate height and ε_0 is the permittivity in a vacuum. For the uniform electric field generation in the plate gap, the electric plate height should be longer than the distance between the gap (h>>d). In this report, we assume the condition as $h = \alpha d$. As a result, the condition of $\alpha > 1$ is required.

3.1.3.3 Relations

We summarize the relations for the important parameters in this section. From the previous discussions, we may select the parameter values, which are the correction angle ϕ, the electric plate length L, the gap distance d and the passage charge Q_l.

At first, the electric field in the gap is restricted by the breakdown. From Eq.(3.1), the electric field is related as

$$E \propto \frac{\phi}{L}. \qquad (3.6)$$

We have an advantage in the cases of the small correction angle and the long kicker plate used. In this project, the pulse duration of kicker is ~100ns, so that the breakdown is assumed as 100kV/cm (=10MV/m).

The voltage required by the trajectory correction is given by

$$U \propto \frac{\phi d}{L}. \qquad (3.7)$$

For the equation, the short distance of the gap has an advantage from the viewpoint of the low voltage required. The voltage is also limited as <1MV for the electrical insulation.

Also, the shot number restricted by the gap switch lifetime is

$$N_s \propto \frac{Q_l}{\phi d}. \qquad (3.8)$$

Consequently, the shot number can be improved by using the gap switch with the large charge transfer, and the small correction angle and narrow distance of the gap. The charge transfer is, for example, 1000C in Ref.[3.4].

3.1.3.4 Results of estimation

(a) Electric field

Figure 3.4 shows the electric field as a function of the correction angle calculated by Eq.(3.1). The correction angle of 20mrad is acceptable in Fig.3.4.

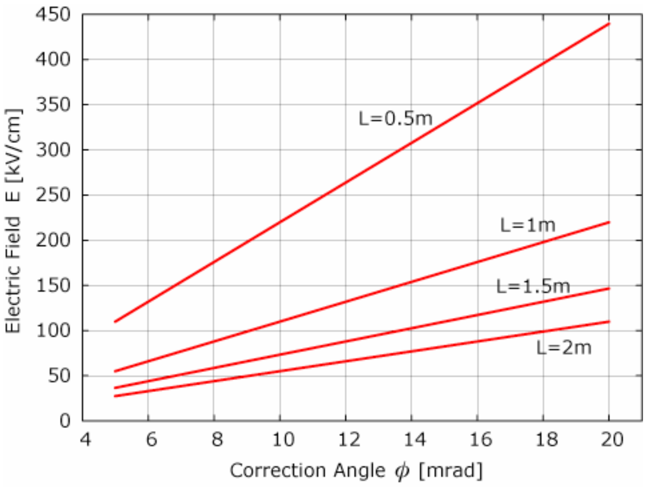

Fig.3.4: Electric field between kicker plates.

(b) Required voltage

Figure 3.5 shows the required voltage as a function of the correction angle given in Eq.(3.2). The narrow gap between the kicker plates can suppress the lower voltage required, however the gap distance should be determined from the beam radius. Considering the beam radius, since the distance of 20cm is required [3.5], the restrictions are L>2m and ϕ<10mrad as shown in Fig.3.5.

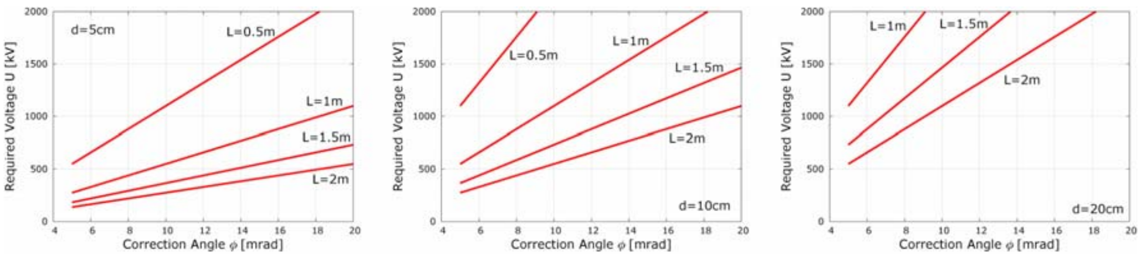

Fig.3.5: Required voltage for electrostatic kicker.

(c) Shot number limitation

From Eq.(3.3), we estimate the relation between the correction angle and the shot number as shown in Fig.3.6. Here the allowable charge transfer Q_l is assumed to be 1C by a conservative estimate. At least, the repetition over 10000 shots can be expected in

Fig.3.6.

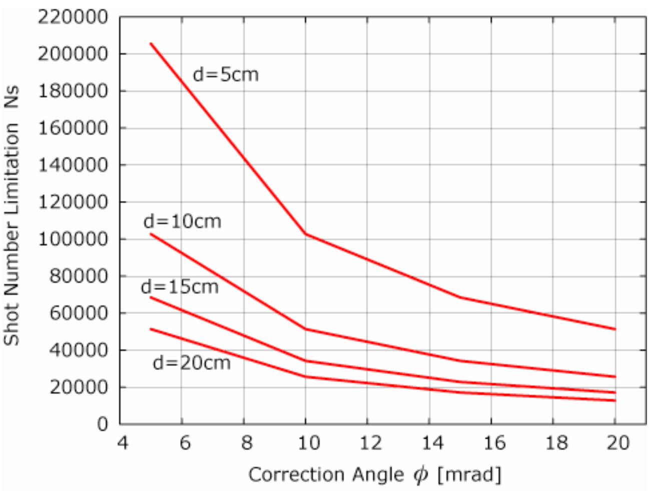

Fig.3.6: Limitation of shot number for gap switch.

3.1.3.5. Summary

In this section, we estimated the electric field, voltage, shot number, for the correction angle and size of the electrostatic kicker plate. The electric field in the gap is restricted by the insulation, but in this case it is not fatal problem because of the short pulse duration. The voltage at one kicker module is limited as <1MV. For this reason, the correction angle at one module is expected as 10mrad at highest. The limitation of shot number is improved by using maintenances of the insulation parts.

3.1.4 Selected momentum correction

By using the individual trajectory correction as discussed in previous section, the trajectory and the divergence angle are corrected, and the emittance can be reduced. However the longitudinal momentum spread of the RI is still remained as large value. For the improvement of the large momentum spread, we proposed the selected momentum correction method [3.1]. In the method, the analyzer detects the RI velocity as TOF, and the induction voltage modulator can correct the momentum error of the RI. The system concept is based on the individual trajectory correction.

4. Cost estimation and schedule

Cost estimation is shown in Table 4.1. And the time schedule is shown in Table 4.2. The estimation shown in Table 4.1 is in the case of the minimum setup plan. The total cost is 1230 Myen. In addition, cost for the upgrade program on individual trajectory correction is estimated to be about 62Myen for electric kickers, switch, laser trigger and particle detectors.

Item		Cost (M yen)	Man power
Isochronous ring	Sector magnets	256 (=8x32)	3
	Power supply for sectors	32(=8x4)	
	Trim coils for harmonic field	4(=8x0.5)	
	Power supply for trim coils	12(=8x1.5)	
	Vacuum system	50	
	Vacuum ducts and stands	70	
	Rf for checking of isochronicity	50	
	Subtotal	**474**	
Kicker and septum	R&D for kicker	3	2
	Kicker magnets	288(=24x12)	
	Septum magnets	100(=2x50)	
	Subtotal	**391**	
Injection line	Retrieve of TARNII	70	1
	Vacuum system	40	
	Vacuum ducts and stands	55	
	Additional Q-magnets	39(=3x13)	
	Subtotal	**204**	
Setup of storage ring and injection line	Setting, wiring, piping etc.	**100**	
Others	NMR probes	32(=8x4)	1
	Particle detectors	24(=24x1)	
	HF cables (130m)	5	
	Subtotal	**61**	
Total		**1230**	7

Table 4.1 Cost estimation and the number of necessary man power for each item. Brackets in the cost estimation columns mean the number of units by the cost of one unit.

<table>
<tr><td colspan="2">Item</td><td>FY1</td><td>FY2</td><td>FY3</td><td>FY4</td><td>FY5</td></tr>
<tr><td rowspan="3">Ring</td><td>Sector magnets</td><td rowspan="2">Conceptual design, Simulations</td><td rowspan="3">Detailed design</td><td rowspan="3">Construction</td><td rowspan="3">Setting, Measuring field map</td><td rowspan="3">Vacuum</td></tr>
<tr><td>Trim coils</td></tr>
<tr><td>RF</td><td></td></tr>
<tr><td rowspan="2">Kicker and septum</td><td>Kicker</td><td>R&D using by model kicker</td><td rowspan="2">Conceptual design, Simulations</td><td rowspan="2">Detailed design</td><td rowspan="2">Construction</td><td rowspan="2">Setting</td></tr>
<tr><td>Septum</td><td></td></tr>
<tr><td colspan="2">Injection line</td><td>Detailed design</td><td>Construction</td><td>Setting</td><td>Vacuum</td><td></td></tr>
<tr><td colspan="2">Others</td><td>R&D</td><td>Construction</td><td>Setting</td><td></td><td></td></tr>
</table>

Table 4.2 Time schedule for sub projects.

References

[2.1] I. Meshkov, et al., Nucl. Instrum. Methods Phys. Res. A 523 (2004) 262.

[2.2] T.Ohkawa, et al., Proceeding of EPAC(2000) Vienna, Austria.

[2.3] T.Ohkawa, et al., Proceeding of EPAC(2002) Paris, France.

[2.4] T.Kubo, Nucl. Intrum. and Meth.in Phys Res. B204 (2003) 97.

[2.5] T.Katayama et al., Part. Accel. 32 (1990) 105.

[3.1] T. Kikuchi, et al., Phys. Rev. ST Accel. Beams 8 (2005) 080402.

[3.2] H. Kumagai, et al., Nucl. Instrum. Methods Phys. Res. A 470 (2001) 562.

[3.3] K. Horioka, *private communications*.

[3.4] SAMTECH PRODUCTS & SERVICES GUIDE, Samtech Ltd. p.17.

[3.5] M. Yamaguchi, et al., Proc. STORI05.